The Influence of Process Parameters on the Properties of PLGA-Microparticles Produced by the Emulsion Extraction Method

Nikolett Kiss and Günter Brenn
Institute of Fluid Mechanics and Heat Transfer, Graz University of Technology, Inffeldgasse 25/F, 8010 Graz, Austria

Daniele Suzzi
Qpunkt GmbH, Gewerbepark 11, A-8075 Hart bei Graz, Austria

Stefan Scheler and Herwig Jennewein
Sandoz GmbH, Sandoz Development Center Austria, Biochemiestrasse 10, A-6250 Kundl, Austria

Juliana Wieser and Johannes Khinast
Research Center Pharmaceutical Engineering, Inffeldgasse 21a, A-8010 Graz, Austria

Controlled release poly(lactic-co-glycolic acid) microparticles for use as active pharmaceutical ingredient carriers were prepared by the emulsion extraction method. Particle formation experiments were carried out in a stirred vessel. The local flow conditions in these experiments, that is, local shear rates and dissipation rates, and the extraction rate of the organic solvent were examined by a computational fluid dynamics (CFD) simulation. The local flow conditions in the stirred tank reactor have a significant influence on the final properties, specific surface area, skeletal density, organic solvent content, and size of the microparticles. We determined nondimensional correlations for predicting these particle properties as functions of the process parameters as, for example, the stirrer speed, emulsion injection point, and oil droplet size in the initial emulsion. The results demonstrate that CFD simulations offer insight into the particle formation process for different batch sizes and provide a basis for scale-up and optimization of the process. © 2012 American Institute of Chemical Engineers AIChE J, 59: 1868–1881, 2013
Keywords: particle technology, mathematical modeling, controlled release formulations, computational fluid dynamics

Introduction

The biodegradable polyesters Poly(lactic acid) and PLGA (Poly(lactic-co-glycolic acid)) are commonly used for delivering active pharmaceutical ingredients (APIs) in a release-controlled manner.[1] They have been assigned the so-called GRAS status, that is, "generally recognized as safe,"—evaluated as biocompatible vehicles for drug delivery and approved by regulatory agencies, such as the Food and Drug Administration and the European Medicines Agency. An API encapsulated in polymer microspheres may be incorporated in controlled-release biodegradable polymers. Various microencapsulation techniques are described in the literature.[2] The classical methods for preparation of microspheres containing active substances are bottom–up techniques. Phase separation (coacervation), spray drying, solvent extraction/evaporation-based processes, and supercritical expansion are methods based on solubility shifts of the polymer. First, a polymer and API are dissolved in a solvent. Next, the polymer is hardened causing the encapsulation of the API in the polymer matrix. Polymer hardening can be performed either by physical means (e.g., addition of antisolvents, temperature changes, solvent extraction) or via chemical reactions in the solution (e.g., polymerization, acid/base shift reaction). In the present work, the microspheres were produced by the emulsion–solvent extraction technique.

Microsphere preparation via solvent extraction basically consists of four major steps[3]: (1) dissolution or dispersion of the bioactive compound, often in an organic solvent containing a matrix-forming material; (2) emulsification of this organic phase in the second continuous (frequently aqueous) phase immiscible with the first one; (3) extraction of the solvent from the dispersed phase via the continuous phase, transforming the droplets into solid microspheres; and (4) harvesting and drying of the microspheres. In this work, the oil-in-water (O/W) emulsification was carried out with an SMX static mixer. We previously reported that the emulsion quality, that is, the mean oil droplet size and droplet size distribution, may be controlled by the process parameters.[4] In that work, we developed a correlation describing the nondimensional oil drop size as a function of the liquid and process properties that allowed to accurately predict a mean oil droplet size.
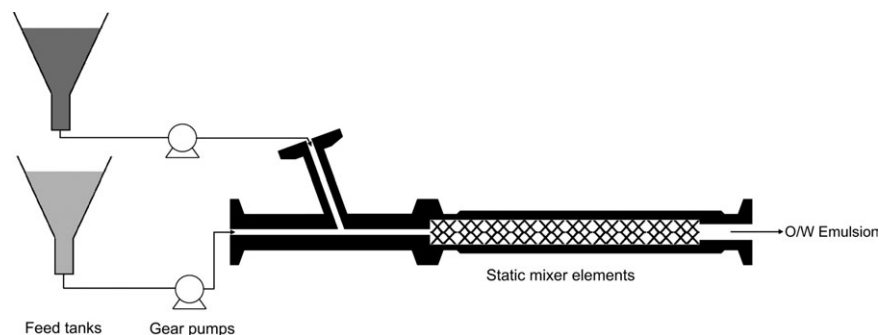
Figure 1. Experimental set-up for the O/W emulsification using a Sulzer SMX static mixer.

The encapsulation technique determines many microparticle properties crucial to API release, including particle size, morphology, porosity, API content, and distribution. All these parameters have been extensively discussed in the literature. In this work, we focus on microparticle properties that can be controlled by the extraction rate and oil droplet size of the emulsion. Polymer and drug properties, such as molecular weight and concentration in the dispersed phase, and API crystallinity were not changed or examined. Process parameters, including surfactant concentration in the continuous water phase and the volume ratio of the different phases, which can also influence the microparticle properties[5] and drug release rate,[6] were kept constant.

Porosity is an essential particle property for manipulating release profiles. The extraction rate during the microparticle preparation via the solvent extraction technique has a direct effect on the final microparticle porosity.[7] The rate at which the solvent is extracted from the droplets of the dispersed phase depends on the flow in the stirred vessel, the droplet size, temperature, and the dispersed phase hold-up in the O/W emulsion. The microparticle porosity and pore size tend to increase with the extraction rate. The initial burst effect, that is, the rapid initial API release in the body, is directly related to the microparticle porosity because the initial release phase is characterized by pore diffusion.[6,8] Therefore, increasing the size and number of pores during the microsphere preparation should increase the release rate of the encapsulated drug.[7,9] A fast solvent removal also affects the shape and surface morphology of polymeric microspheres. It was established that fast extraction leads to irregularly shaped microparticles, with indentations in their surface.[10] Furthermore, quick solvent extraction was shown to be responsible for interfacial polymer deposition and to lead to the formation of hollow, core-shell-like microspheres.[11] The effects of a temperature gradient or dilution of the continuous phase during solvent removal are also discussed in the literature.[12,13] Fast solvent removal using a temperature gradient resulted in microspheres with a hollow core and high residual solvent content. Slower and gradual solvent removal using dilution of the continuous phase resulted in a uniform porous structure without core.[13] The dependence of the interparticulate pore-size distribution of microspheres on the solvent extraction temperature was also investigated using the solvent extraction/evaporation process.[12] The microspheres prepared at lower temperatures had a coarse pore structure with large pores embedded in a tightly packed polymer matrix. Due to the slow and incomplete solvent extraction at low temperatures, only a small fraction of micropores was observed. However, during faster extraction at higher temperatures, a densified shell was formed around the particles.

Particle-size distribution is another important factor affecting the drug release profile. For example, it has an impact on the encapsulation efficiency in the polymer matrix of PLGA.[14] Smaller microspheres showed a lower drug content due to their high specific surface area. Moreover, the drug release rate was found to increase with the decreasing microparticle size.

As stated earlier, parameters such as porosity, particle size, and API distribution in relation to the release behavior of controlled release microspheres have previously been studied. Nonetheless, the influence of the process parameters of the emulsion extraction technique on the aforementioned particle properties has scarcely been investigated. In addition, scale-up is often a problem because the final particle properties strongly depend on the formation parameters related to the batch size. In this work, we incorporated results from flow simulations into the analysis of particle formation experiments. Computational fluid dynamics (CFD) enhances the understanding of the flow in an extraction vessel used for the production of the polymeric microparticles. Establishing the local dissipation, shear, and extraction rates at different agitator speeds and droplet injection points helps to understand the micromixing of the emulsion at the injection point. As it appears, the micromixing of the emulsion at the smallest scales of turbulence is a crucial factor influencing the final properties of the polymeric microparticles. CFD simulations offer insight into the particle formation process for different batch sizes and provide a basis for the scale-up and optimization of the process.

The present article is organized as follows: the next section introduces the materials, experimental set up, and particle characterization methods used. Then, the nondimensional representation of the particle properties specific surface area, skeletal density, residual organic solvent content, and particle size is developed by dimensional analysis. In the next section, the flow simulations are presented. After that, the experimental design is described. In the next section, the experimental results are presented with an analysis of the influences of the various experimental parameters on the particle properties. The article ends with the conclusions.

Materials and Methods
Materials and microparticle preparation technique

Microparticles were prepared by the emulsion solvent extraction technique. The O/W emulsion was prepared by the experimental set-up shown in Figure 1. The two immiscible liquids, the dispersed and continuous phases of the emulsion, were transported from their feed tanks by gear pumps

Table 1. Material Properties of the Dispersed and Continuous Phases of the Emulsion and of the Extraction Medium

	Dispersed Phase	Continuous Phase	Extraction Medium
ρ (kg/m^3)	994.8	999.9	998.2
μ (kg/ms)	0.1740	0.0032	0.00152

(Ismatec IP65) and forced through a static mixer. The SMX static mixer elements were provided by Sulzer ChemTech and were fitted in a specific housing tube. The tube contained 10 mixer elements with 6 mm length and diameter. The total length of the mixing zone was 6 cm. The fluid velocity in the static mixer was 7.5×10^{-2} m/s and 1.6×10^{-1} m/s, depending on the desired oil droplet size. A detailed description of the emulsification apparatus and technique is presented in our previous publication.[4] The continuous phase of the emulsion was a mixture of deionized water and poly(vinylalcohol) 26-88 (PVA), purchased from VWR, dissolved as the emulsifier. For the preparation of the continuous phase, the deionized water was heated to 80°C, and 1 wt % of solid PVA was dissolved. The liquids constituting the organic dispersed phase of the emulsion were ethyl acetate and benzyl alcohol, both from VWR. The volume ratio of benzyl alcohol and ethyl acetate in the dispersed phase was 0.5. Poly(D,L-lactide-co-glycolide) with the polymer composition of 75:25 (molar ratio of D,L-lactide:glycolide) (Resomer RG 757 S) was purchased from Boehringer Ingelheim (Germany). This PLGA polymer was dissolved in the ethyl ace-

tate (0.111 g/mL). The mean molecular weight of this polymer is $M_w = 64,710$ Da. The API, 3-{2-[4-(6-fluor-1,2-benzisoxazol-3-yl)piperidino]ethyl}-2-methyl-6,7,8,9-4-H-pyrido[1,2-a]pyri- midin-4-one was obtained from Jubilant Organosys (India). The API was dissolved in the benzyl alcohol (0.34 g/mL). The PLGA polymer solution in ethyl acetate and the API solution in benzyl alcohol were then mixed. The total 60 mL of the organic mixture constituted the dispersed phase of the emulsion, which was dispersed in 635 mL of the aqueous phase. The density and dynamic viscosity of the dispersed and continuous phases of the emulsion are listed in Table 1.

The O/W emulsion was directly fed into a 5-L jacketed Schmizo batch reactor containing 3.5 L of the extraction medium using a glass tube with the inner diameter of 7 mm. The inner diameter of the reactor was 180 mm and the diameter of the anchor agitator was 112 mm. The extraction medium was deionized water with 2.4 wt % ethyl acetate. Its density and dynamic viscosity are also listed in Table 1. The oil droplets of the emulsion were transformed into solid microparticles by solvent extraction (stirring for 20 h at 5°C). Different particle formation experiments were performed by varying the stirring speed, mean oil droplet size of the emulsion, and position of the injection point of the emulsion. Figure 2 shows the experimental set-up of the extraction step, indicating the two emulsion injection points. At the end of the extraction step, the solid microparticles were separated by filtration using a filtration funnel with integrated sintered glass filter disc (DURAN Group, Porosity 1) and dried with an air flow at 5°C.
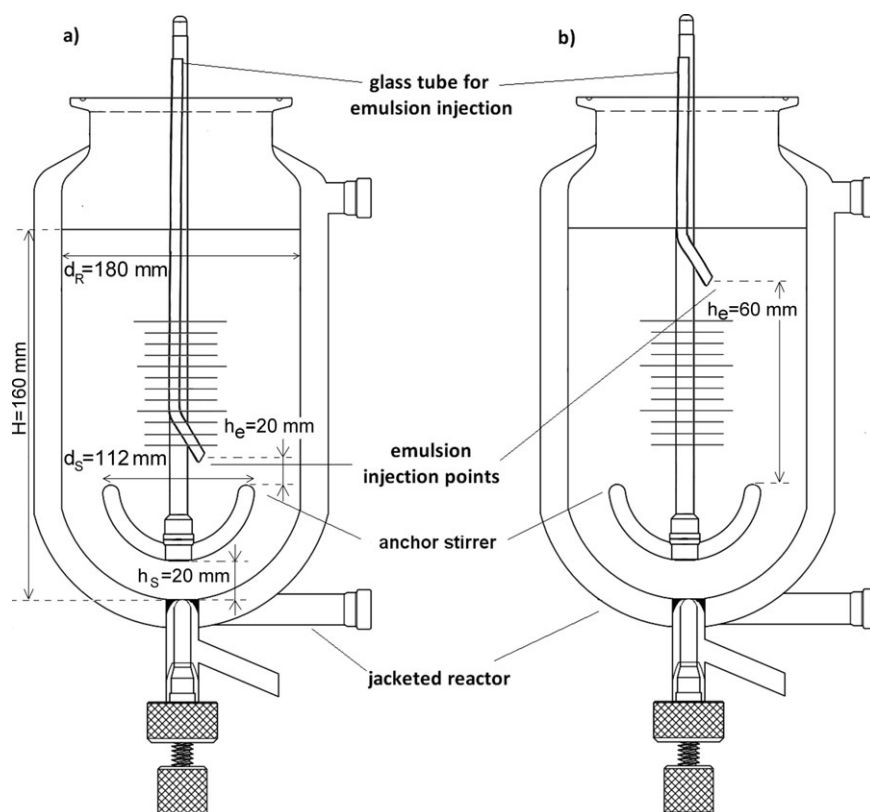

Figure 2. The 5-L Schmizo-jacketed glass reactor for solvent extraction equipped with an anchor stirrer and a glass tube for emulsion injection.

The emulsion was fed into the extraction medium at two different injection points; the vertical distances h_e between the injection point and the stirrer tip were (a) 20 mm and (b) 60 mm.

After drying, the particles were suspended in a washing solution, a mixture of deionized water, and 25 vol % ethanol. This ethanol solution was used to prevent agglomeration of the microparticles and to further reduce their residual organic solvent content. Ethanol was purchased from Lactan (Austria). All solvents were used in their original states. By stirring at 180 rpm for 6 h, the particles were washed in 4 L of washing solution in the same 5 L glass reactor at 25°C. At the end of the process, the particles were filtered again and dried with an air flow at ambient temperature.

Analytical methods

Oil Droplet and Particle Size Measurement by Laser Diffraction Spectrometry. The oil droplet size spectra of the O/W emulsion[4] and the particle size spectra of the produced microparticles and their Sauter mean diameters d_{32} were measured using a laser diffraction instrument Sympatec HELOS, H2395. After 20 h of extraction, a sample containing the dispersed hardened particles was collected from the extraction medium. The particle dispersion was analyzed undiluted, immediately after sampling. A 50-mL glass cuvette provided by Sympatec with the Fourier optics R5 (particle size measuring range 0.5/4.5 … 875 μm) was used as the particle disperser. All samples were measured in triplicate.

The particle-size distribution is determined as a volume fraction of particles q_3^* in the ensemble, which is common in diffraction-based sizing techniques. The Sauter mean diameter is determined as a characteristic particle size, defined as

$$d_{32} = \frac{\Sigma_i N_i d_i^3}{\Sigma_i N_i d_i^2} \quad (1)$$

where N_i is the number of particles with the diameter d_i.

The volume-based size spectrum and the Sauter mean diameter of the oil droplets $d_{32,\text{oil}}$ were also determined using the HELOS instrument. The diffraction patterns were evaluated in the mode Fraunhofer Enhanced Evaluation of the instrument's data processing software.

Scanning Electron Microscopy. The internal structure and composition of the microparticles were studied by scanning electron microscopy (Zeiss Ultra 55, Carl Zeiss NTS GmbH, Oberkochen, Germany) and energy dispersive x-ray analysis (EDAX Genesis, EDAX, Mahwah). To visualize their internal structure, the particles were placed on a liquid-nitrogen cooled plate and cut with a scalpel. Subsequently, the specimens were coated with a thin carbon layer (~20 nm thickness).

Residual Solvent Content Measurement by Gas Chromatography. The residual content of ethyl acetate, benzyl alcohol, and ethanol in the microparticles was measured by gas chromatography, using the Perkin–Elmer Clarus 500 instrument equipped with a flame ionization detector and liquid autosampler. The mobile phase was nitrogen. The stationary phase was an Optima-5 MS capillary column (Macherey-Nagel, 30.0 m × 320 μm × 0.25 μm nominal). The total amount of residual solvent w_{res} of the microparticles was calculated in wt %.

Specific Surface Area and Skeletal Density Measurements. The specific surface area of the samples was determined by the Brunauer–Emmett–Teller (BET) method using the surface analyzer Tristar II 3020 from Micrometrics. Before the measurements, the samples were dried with a nitrogen gas flow for 1 day. The measuring gas was krypton, and the specific surface area was calculated with the data processing software of the instrument.

The skeletal density of the samples was measured by helium pycnometry, using the instrument AccuPyc II 1340 from Micrometrics.

Dimensional Analysis

Dimensional analysis was used to develop correlations of the four particle properties specific surface A_{spec}, skeletal density ρ_{sk}, residual solvent content w_{res}, and Sauter mean diameter d_{32} with relevant process parameters and material properties.

The underlying assumption is that the particle properties can be expressed as functions of the parameters relevant for particle formation.[15] The four aforementioned particle properties are predominantly determined by mass transfer between the oil droplets of the emulsion (which turn into particles) and the extraction medium. For describing mass transfer in the liquid–liquid extraction process for microparticle formation, the following parameters were considered relevant: the mean oil droplet size $d_{32,\text{oil}}$, the diffusion coefficients of the organic solvent in the dispersed phase and in the extraction medium, and the density ρ and dynamic viscosity μ of the extraction medium. Because the composition of the dispersed phase was kept constant in all experiments, the diffusion coefficient of the organic solvent in the dispersed phase did not vary. This quantity is, therefore, not relevant for the dimensional analysis. Because the extraction medium was also the same in all experiments, the diffusion coefficient of the organic solvents in the medium did also not change. Because this diffusion coefficient D, however, is relevant for the convective mass transfer across the particle surface, D was used as a scaling factor in the analysis. The convective mass transfer is, furthermore, determined by the turbulent flow in the extraction medium relative to the particle motion. The local shear rate $\dot{\gamma}$ and the dissipation rate of turbulent kinetic energy ε may be taken as relevant characteristics of the flow field, where the question remains if the particle properties are determined by the local values of these quantities at the emulsion injection point, or by their global averages in the stirred reactor. Both the shear rate and turbulent dissipation rate in the flow field depend on the stirring speed. Having established the correlations for the particle properties, the question about the importance of local or global turbulent flow field properties for the particle formation may be answered.

The dimensional analysis for the four particle properties, with ε as the relevant turbulent flow property of the extraction medium, involves six dimensional quantities and three basic dimensions and, therefore, leads to three nondimensional groups for each particle property. The four following model equations are obtained.

$$\frac{A_{\text{spec}}\mu}{d_{32,\text{oil}}^{1/3}\varepsilon^{1/3}} = BSc^c \left(\frac{\varepsilon d_{32,\text{oil}}^4}{D^3}\right)^d \quad (2)$$

$$\frac{\rho_{sk}\varepsilon^{1/3}d_{32,\text{oil}}^{4/3}}{\mu} = ESc^f \left(\frac{\varepsilon d_{32,\text{oil}}^4}{D^3}\right)^g \quad (3)$$

$$\frac{w_{\text{res}}D^3}{\varepsilon d_{32,\text{oil}}^4} = HSc^k \left(\frac{\varepsilon d_{32,\text{oil}}^4}{D^3}\right)^m \quad (4)$$

$$\frac{d_{32}\,\varepsilon^{1/4}}{D^{3/4}} = NSc^p \left(\frac{\varepsilon d_{32,\text{oil}}^4}{D^3}\right)^q \quad (5)$$

In these equations, $Sc = \nu/D$ is the Schmidt number of the extraction medium. The coefficients B, E, H, and N, and the exponents c, d, f, g, k, m, p, and q of these model equations are determined by fitting the equations to the results of the particle formation experiments using nonlinear regression. The resulting correlations will be presented in a later section.

Flow Simulations

The properties of the flow field of the extraction medium in these experiments (i.e., time-average velocities, local shear rates and dissipation rates) and the extraction rate were examined by CFD simulations.

The numerical simulations of the stirring and extraction processes were performed using the CFD code FIRE release 2009.1.[16] Based on a Reynolds-averaged Navier–Stokes approach, transient incompressible calculations of the flow in the glass reactor were performed. The finite volume mesh consisted of around 550,000 cells with an average cell size of around 2 mm. To describe the rotation of the impeller, the sliding mesh model was used. In this method, the computational mesh is separated into rotor and stator grids for the domain that includes the impeller and the tank walls. The rotor mesh physically moves during the calculation and flow data are transferred at each time step between the domains. The free liquid surface on the top of the liquid bath was assumed to be flat, with a slip-wall boundary condition. The geometry of the injection glass tube was not considered, that is, the flow around the submerged glass tube during emulsion injection was disregarded, in agreement with the experimental practice prescribing that the glass tube should be removed from the vessel after dosing the emulsion. Further details of the numerical approach and its experimental validation can be found in the literature.[17]

Turbulence was modeled using the k-ζ-f approach,[18] where k is the turbulent kinetic energy, ζ is the normalized velocity scale ratio, and f the elliptic relaxation function. The formulation of this general low-Reynolds-number eddy-viscosity model, which is based on Durbin's elliptic relaxation concept,[19] is similar to the standard k-ε model. However, we modified it by including nonlocal pressure-strain effects and near-wall turbulence anisotropy to adapt the wall functions.

In our model, the velocity scale ratio is related to the squared velocity scale $\bar{v}^2$ and the turbulent kinetic energy k as per

$$\zeta = \bar{v}^2/k \tag{6}$$

Here, the velocity scale $\bar{v}^2$ describes the velocity fluctuations normal to the cell velocity vector and represents the turbulent damping close to the wall. The eddy viscosity ν_t in the formulation of turbulent stresses is expressed as

$$\nu_t = C_\mu \zeta \frac{k^2}{\varepsilon} \tag{7}$$

where C_μ is a model coefficient and ε is the dissipation rate of the turbulent kinetic energy. Numerically, this three-equations turbulence model solves the transport equation for ζ, together with the standard k and ε equations.

To resolve the emulsion flow and extraction process in the stirred tank, the Lagrangian discrete particle method approach, also known as the Lagrangian Monte Carlo method,[20] was used, under which groups of real particles, termed parcels, are statistically tracked in the physical, velocity, and particle-

diameter spaces. Submodels for drag, turbulent dispersion, and extraction were included in our simulations. Under this method, each physical phenomenon occurring in a parcel, for example, mass transfer, directly applies to all the particles in the parcel, resulting in a drastic reduction of the computational effort. In this work, we neglected the effects of collisions among droplets, which was valid because the volume fraction of the injected emulsion was low. Droplet deformation was neglected as well. The particle drag was formulated by a standard drag coefficient model for spherical particles as a function of the particle Reynolds number ($C_D = 24(1 + 0.15\,Re_p^{0.687})/Re_p$ for $Re_p < 10^3$, and $C_D = 0.44$ for $Re_p > 10^3$). In the computation of the particle Reynolds number Re_p, both the difference between the time-average liquid and particle velocities, and the turbulent velocity fluctuations were accounted for. Due to the short Stokesian relaxation time of the particles, the velocity fluctuations dominate the transport processes across the particle interface. Details of the turbulent dispersion modeling can be found in the literature.[17] Because the concentration of the emulsion droplets in the stirred tank was low, it was appropriate to use one-way momentum coupling between the continuous fluid and the parcels.

The mass transfer rate, and, thus, the rate of extraction of the organic solvent from the disperse phase, is basically a function of the equilibrium solubility of the solute, the specific surface of the droplets, the concentration of the dissolved material, the diffusion coefficient in the liquid phase, and the relative velocity between the droplets and the fluid. In our simulations, the mass transfer rate for each droplet was described by the following equation[21,22]

$$\dot{m}_{Extr} = \frac{Sh\,D}{d_{32,oil}} A M (c_S - c_\infty) \tag{8}$$

The quantities in Eq. 8 are the diffusion coefficient D of the organic solvent in water, the Sauter mean oil drop diameter $d_{32,oil}$ and surface A, the molar mass M of the extracted solvent, the saturation concentration c_S of the extracted medium on the surface of the disperse phase and concentration c_∞ in the cell containing the parcel. The concentrations c_S and c_∞ are molar concentrations. For the saturation concentration, the value for EA in water at 5°C was taken from the literature.[23] The concentration c_∞ of the extracted substance is computed for each cell by means of the transport equation for the mixture component EA.

The Sherwood number Sh is calculated using the Frössling equation as a function of the particle Reynolds and Schmidt numbers, Re_p and Sc, respectively.

$$Sh = 2 + 0.552\sqrt{Re_p}\,Sc^{1/3} \tag{9}$$

The particle Reynolds number Re_p in Eq. 9 was based on the oil drop Sauter mean diameter as the length scale and on the relative velocity between the oil drops and the extraction medium as the velocity scale. In turbulent flow, the relative velocity is given by the difference between the time-average drop and extraction medium velocities plus the contribution from the turbulent fluctuations. This relative velocity may be empirically represented by the Kolmogorov velocity given by the tip speed v_0 of the stirrer and the ratio $(d_{32,oil}/d_S)^{1/3}$ as in the equation[24]

$$\mathrm{Re}_P = \frac{v_{\mathrm{rel}} d_{32,\mathrm{oil}}}{v} = \frac{v_0 \left(\frac{d_{32,\mathrm{oil}}}{d_S} \right)^{1/3} d_{32,\mathrm{oil}}}{v} = \frac{\pi n d_S \left(\frac{d_{32,\mathrm{oil}}}{d_S} \right)^{1/3} d_{32,\mathrm{oil}}}{v}$$

$$(10)$$

The quantity d_S is the diameter of the stirrer.

Experimental Design

As stated previously, the microparticle properties depend on the parameters of the particle formation process. Properties of turbulence, such as turbulence intensity, rate of dissipation of turbulent kinetic energy, or a local, time-average shear rate, may be considered as influential on the processes of mass transport across the particle-liquid interface, that is, on the particle formation. Because the geometry of the flow field in the reactor is fixed in our study, and the liquid properties do not vary in the different experiments, these turbulent flow field properties and their spatial variability may be related to the stirring speed only. On the basis of this assumption, the following process parameters were considered important for the extraction, and, therefore, varied in the experiments: the stirring speed n, position of the injection point of the emulsion h_e, and the mean oil droplet size of the emulsion $d_{32,\mathrm{oil}}$.

Particle formation experiments were carried out at three stirring speeds (100, 180, and 260 rpm) and with two initial mean oil droplet sizes of the emulsion. For the point of injection of the emulsion, two different locations—close to the agitator and far away from it—were chosen. The experimental parameters are listed in Table 2.

At different stirring speeds, different local turbulent kinetic energies are realized in the extraction medium. In Experiments 4 and 7, the mean oil droplet size of the O/W emulsion was 29% smaller than in all the other cases. This change in the oil drop size is achieved by an increased flow velocity through the static mixers.[4] In Experiments 1, 2, 3, 5, and 6, the fluid velocity in the static mixer was 7.5×10^{-2} m/s, whereas in Experiments 4 and 7, it was increased to 1.6×10^{-1} m/s. The respective oil droplet size spectra obtained by laser diffraction are shown in Figure 3. The oil droplet size spectrum of the emulsion is a determining factor for the rate of mass transfer between the oil phase and the extraction medium, that is, the rate of solvent removal.

Furthermore, we investigated the influence of the emulsion injection point on the particle properties. In the first set of experiments, the distance between the end of the glass tube for emulsion injection and the level of the blade tip of the anchor stirrer was 20 mm (Figure 2a). In the second set of experiments, the glass tube end was positioned at a distance of 60 mm from the stirrer (Figure 2b). The two injection positions correspond to the different local liquid flow field properties listed in Table 3 below. After dosing the emul-
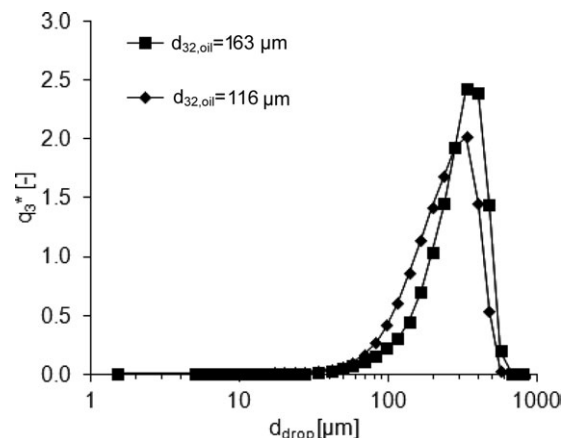

Figure 3. Volume-based oil droplet size spectra of oil-in-water emulsions with Sauter mean diameters of 163 and 116 μm; the emulsion with larger oil droplet size was used in experiments 1,2,3,5, and 6, and the emulsion with the reduced mean oil droplet size was used in the Experiments 4 and 7.

sion, the glass tube was removed from the reactor, and the extraction was carried out in a closed system.

Results and Discussion

Results of the flow simulations

Examples of the time-average velocity field in a meridional plane of the flow field for the three different stirring speeds are presented in Figure 4. As pointed out above, the fluid flow around the injection tube was not considered. The computed data form a basis for the representation of the influences of the flow field on the final particle properties. Spatial distributions of turbulent properties of the flow field, such as the dissipation rate and shear rate, are a part of these results, not shown here in diagrams. Local values at the emulsion injection point and global volume-average values for the whole reactor of the shear rate and the turbulent dissipation rate are given in Table 3. The local values are computed as averages along a circle around the symmetry axis of the vessel through the orifice of the glass tube.

Making use of these results, the transient extraction process was computed for the first seconds after the start of injection. The diagram in Figure 5 shows the increase of ethyl acetate mass in the reactor with time for the seven experimental situations listed in Table 2. A second-degree polynomial $m = \frac{1}{2}at^2 + bt + c$ was fitted to each series, and the coefficient a, which is the curvature of the parabola and a time-independent characteristic of the rate of

Table 2. Parameters of the Seven Particle Formation Experiments

Experiment No.	n (1/s)	h_e (cm)	$d_{32,\mathrm{emulsion}}$ (μm)
1	4.33	2	163
2	1.67	2	163
3	3	2	163
4	3	2	116
5	3	6	163
6	4.33	6	163
7	1.67	6	116

Table 3. Local and Global Average Shear Rates and Dissipation Rates, and the Coefficient a Characterizing the Extraction Rate

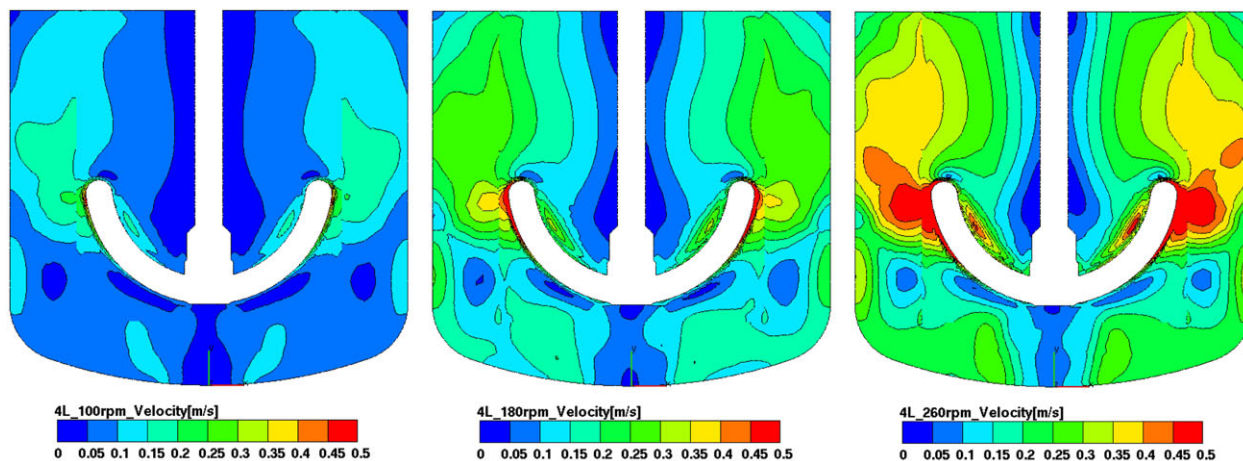| Experiment No.	$\dot{\gamma}_{\mathrm{loc}}$ (1/s)	$\varepsilon_{\mathrm{loc}}$ (m²/s³)	$\dot{\gamma}_{\mathrm{vol}}$ (1/s)	$\varepsilon_{\mathrm{vol}}$ (m²/s³)	a (mg/s²)
1	16.4	0.03722	24.02	0.0526	0.1044
2	6.6	0.00257	9.57	0.0033	0.0418
3	11.4	0.01274	16.94	0.0178	0.074
4	11.4	0.01274	16.94	0.0178	0.163
5	8.2	0.00342	16.94	0.0178	0.0876
6	12.0	0.01054	24.02	0.0526	0.146
7	4.4	0.00052	9.57	0.0033	0.3658

Figure 4. Velocity distribution in a meridional plane of the reactor for (left to right) 100, 180, and 260 rpm.

[Color figure can be viewed in the online issue, which is available at wileyonlinelibrary.com]

extraction, was used as a measure of the extraction process kinetics. The initial condition determines that the coefficient c is zero. The purpose of this calculation was to produce constant characteristic values for the various time-dependent experimental situations. The results are shown in Table 3 together with the turbulent flow field properties.

Particle size, specific surface area and skeletal density

The size spectra of the hardened microparticles were measured after the extraction step. In Experiments 4 and 7, the Sauter mean diameter of the particles was 30 and 49 μm, respectively, whereas in Experiments 1, 2, 3, 5, and 6 particles with Sauter mean diameters between 117 and 141 μm were produced. The particle-size distributions are given in Figure 6 for all seven experiments. In Experiments 4 and 7, the Sauter mean diameter of the particles was decreased, and the fraction of large oil droplets was reduced by changing the parameters of the O/W emulsification.[4] Increasing the flow velocity in the emulsification apparatus led to reduced particle sizes and broader particle-size distributions.

In Experiments 1, 2, 3, 5 and 6, the initial mean oil droplet size of the emulsion is 163 μm. However, in Experiment 1, the observed particle size was 117 μm, that is, signifi-

cantly smaller than 163 μm. This can be explained by the high stirring speed (4.33 s^{-1}) and by the highest local shear rate (16.4 s^{-1}) in this experiment. The high stirring speed and the emulsion injection point placed near the blade of the anchor stirrer may have caused droplet deformation and breakup at the injection tube. The break-up of the oil droplets led to reduced particle sizes, broader particle-size distributions (Figure 6), and the formation of irregular polymer precipitates. The mean particle size d_{32} and distribution
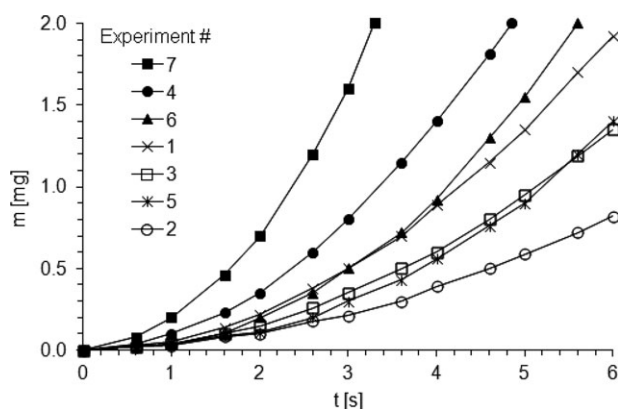

Figure 5. Ethyl acetate mass m in the reactor as a function of time during the first few seconds of the extraction from simulated mass transfer based on properties of the liquid flow field in the reactor.
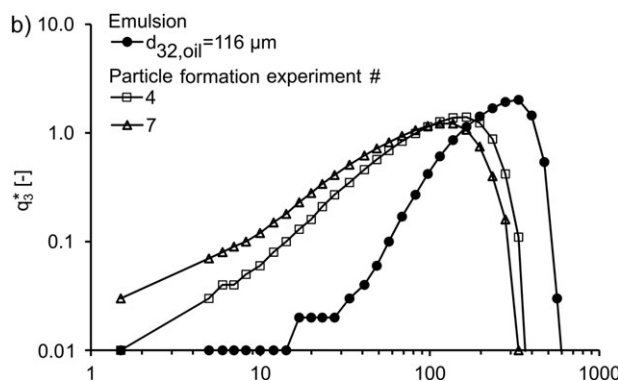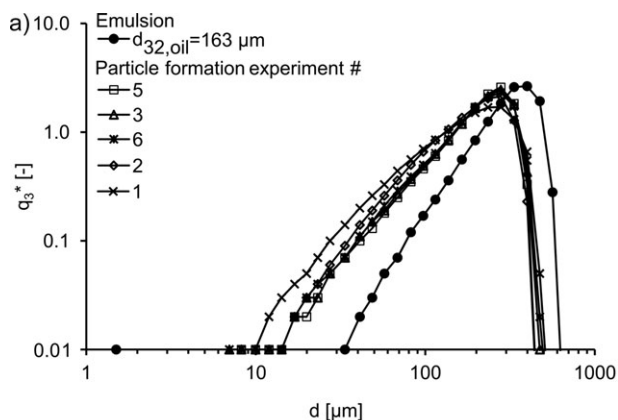

Figure 6. Volume-based particle size spectra for all microparticle formation experiments.

(a) Formulations using the initial mean oil droplet size $d_{32,oil}$ = 163 μm and (b) formulations using the initial mean oil droplet size $d_{32,oil}$ = 116 μm.

Table 4. Sauter Mean Oil Droplet and Particle Size, and the Particle Size Distribution Width

Experiment No.	$d_{32,oil}$ (μm)	d_{32} (μm)	SPAN
1	163	117	1.38
2	163	135	1.20
3	163	137	1.12
4	116	49	1.73
5	163	141	1.08
6	163	134	1.17
7	116	30	2.01

Particles were measured after solvent extraction.

width data are summarized in Table 4. The particle-size distribution width (SPAN) can be described by the equation

$$SPAN = (d_{90} - d_{10})/d_{50} \qquad (11)$$

where the diameters d_{10}, d_{50}, and d_{90} are properties of the cumulative particle-size distribution.

As can be seen from Figure 6, the particle size is a function of the oil droplet size of the emulsion produced as a particle precursor. The oil droplet size may have been altered by droplet breakup during the injection into the extraction medium as a consequence of the liquid flow field in the extraction vessel as described above. The final microparticle size and the specific surface area of the particle ensemble have a significant influence on the erosion of polymeric microparticles during dissolution and, therefore, on the release rate of the API.

Because of the fast microparticle hardening during solvent removal, deformation and break-up of the droplets can only occur immediately after start of extraction, that is, close to the emulsion injection zone. Nevertheless, the question remains if the micromixing of the emulsion at the smallest scales of turbulence, or the macromixing at the scale of the vessel is crucial regarding the final particle properties. Therefore, both the flow situation at the emulsion injection point and the global turbulent flow field should be considered in the analysis. The parameters obtained from the simulations can contribute to a better understanding of the process. From the local energy dissipation rates, the Kolmogorov length-scale can be calculated as

$$\lambda = \left(\frac{v^3}{\varepsilon_{loc}} \right)^{1/4} \qquad (12)$$

where v is the kinematic viscosity of the extraction medium. The calculated values of the Kolmogorov size λ and the initial mean oil droplet sizes of the emulsion are summarized in

Table 5. The estimated Mean Oil Droplet Size, Kolmogorov Length-Scale, Particle Reynolds Number, Sherwood Number, Mass Transfer Coefficient $\beta = ShD/d_{32,oil}$ and Agitator Reynolds Number, Estimated by Eqs. 9, 10, 12, and 13

Experiment No.	$d_{32,oil}$ (μm)	λ (μm)	Re_P (−)	Sh (−)	β (m/s)	Re_S (−)
1	163	98	18.5	31	0.000160	35,697
2	163	193	7.1	20	0.000103	13,730
3	163	129	12.8	26.1	0.000134	24,713
4	116	129	8.2	21.2	0.000154	24,713
5	163	179	12.8	26.1	0.000134	24,713
6	163	135	18.5	31	0.000160	35,697
7	116	287	4.5	16.3	0.000118	13,730

The Sc number of the extraction medium is 1809.

Table 5. One can see that, in Experiments 1, 3, and 6, the estimated Kolmogorov length scales are smaller than the initial mean oil droplet size used as a particle precursor. In these experiments, droplet deformation by interaction with the liquid turbulence after emulsion injection may be effective on the droplet size. In Experiments 4 and 5, λ is nearly of the same size as $d_{32,oil}$. In Experiments 2 and 7, the Kolmogorov length scale is in both cases larger than the oil droplet size. Due to the mild local flow situations, droplet breakup is not probable in these experiments.

The estimated values of the various quantities are summarized in Table 4. We also include the agitator Reynolds number. This dimensionless number is defined as

$$Re_S = \frac{nd_S^2 \rho}{\mu} \qquad (13)$$

Previous investigations have shown that the properties of PLGA microparticles can be influenced by the process parameters.[25–27] From Table 5, it is obvious that the parameters discussed above are modified by the stirrer speed n and the oil droplet size $d_{32,oil}$ in our experiments. The location of the injection is not considered in these values. However, as stated earlier, the location of the emulsion injection has a significant role, if droplet breakup occurs. Therefore, in our analysis, the parameter ε was used instead of the values Re_P, Sh and β. In our opinion, the use of the value ε provides a better description of the extraction process.

The BET surface area A_{spec} of the particles in the samples and the particle Sauter mean diameter are given in Figure 7. A large mean particle size is accompanied by a small specific surface area of the particles and vice versa. The relation between the BET surface area A_{spec} and the coefficient a is shown in Figure 8. Because the particle–liquid mass transfer is a function of the particle size, and as the BET surface area is smaller for larger particles, the coefficient a inversely depends on the particle size and follows the same trend as the BET surface area.

The results of the skeletal density measurements are shown in Figure 9. To establish a relationship between the flow conditions in the extraction vessel and the skeletal density data, the local dissipation rate is plotted in the same diagram. A trend is not readily seen, and, in the whole set of
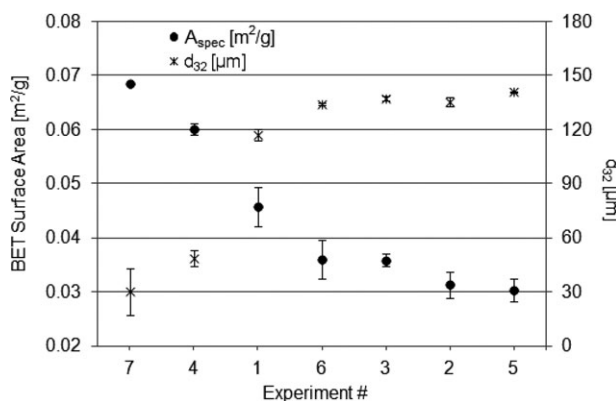
Figure 7. The BET surface area A_{spec} and the Sauter mean particle size d_{32} for all microparticle formation experiments.

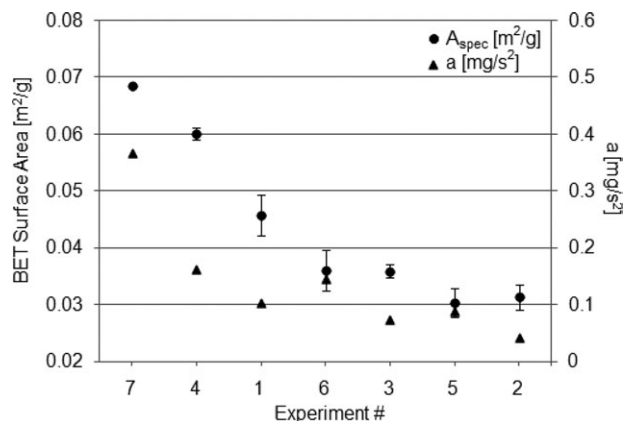See Tables 2 and 3 for experimental details.

Figure 8. Specific surface area of the microparticles A_{spec} and the coefficient a calculated by flow simulations.

See Tables 2 and 3 for experimental details.

experiments, the values of ρ_{sk} vary by no more than 1.4%. The particles with higher skeletal densities were produced when the emulsion was injected close to the anchor stirrer (Experiments 1–4). At lower local shear rates at the injection point, particles with lower skeletal density are produced. This phenomenon may be due to the strong influence of the solidification rate on the particle morphology.[13] Quick solvent extraction occurs when the Sherwood number of mass transfer Sh_P is high. The dimensionless number Sh_P depends on the Reynolds and Schmidt numbers, Re_P and Sc. Slow solidification generally leads to high porosity. The soft state of microparticles is extended and, due to the delayed hardening, a homogeneous polymer matrix with pores and channels is created. Fast solvent removal leads to lower surface area, denser periphery, and higher residual solvent content.[11]

Residual solvent content

The residual solvent content w_{res} in the microparticle samples and the local dissipation rates ε_{loc} are given in Figure 10. If we look at the results related to the same stirrer speed (Experiments 1 and 6 for 4.33 s^{-1}; Experiments 2 and 7 for 1.67 s^{-1}; Experiments 3, 4 and 5 for 3 s^{-1}), we can conclude that microparticles produced at higher local dissipation rates in the extraction medium have a higher residual solvent content than those produced at lower local dissipation rates at the
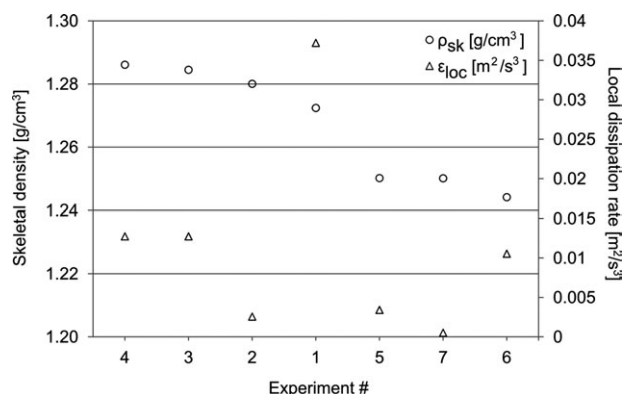
same stirrer speed. A higher organic solvent concentration in the final solid microparticles may be due to the fast solvent removal at higher dissipation rates near the anchor stirrer. It is known that fast solvent removal can result in early polymer precipitation in the periphery region of the microparticles,[11] thus reducing the extraction rate at later times.

It is reasonable to conclude that the high skeletal density of Samples 1, 2, 3, and 4 (Figure 9) is related to the higher residual solvent content in these samples. Fast extraction and polymer precipitation in the near-surface region of the particles results in a reduced over-all solvent removal and, therefore, in a higher organic solvent content in the particles. Because the final size distributions of the microparticle Samples 2, 3, 5, 6, and 4, 7 are very similar (Figure 6), the differences in the skeletal density may be related to the different residual solvent content. More residual organic solvent means denser particles, that is, higher skeletal density.

The specific surface area (Figure 8), the skeletal density (Figure 9), and the residual solvent content (Figure 10) of the Samples 1, 6 and 3, 5 and 2, 7 are different. The Experiments 1, 6 and 3, 5 and 2, 7 differ only in the emulsion injection point. As discussed in the preceding section, the particle size and specific surface area are strongly related (Figure 7). These two parameters can be correlated with the coefficient a, which is a quantity characteristic of the first seconds of the extraction process (Figure 8). Skeletal density and residual solvent content of the microparticles can be correlated with the local dissipation rate (Figures 9 and 10). Our interpretation is that the particle size and specific surface area are affected by the rate of extraction, that is, the drop size evolution is a long process influenced by the temporal extraction profile. With regard to particle size, the local flow conditions may induce drop breakup immediately after the droplet injection. Residual solvent content and skeletal density are particle properties determined immediately after the emulsion injection and strongly depend on the flow at the emulsion injection point.

An interesting quantity to note is the yield of the extraction process. For quantifying this, we computed the degree of reduction of organic solvent content from the oil droplet state to the final particles. For doing this, we calculated the mass content of organic solvents of the oil droplets in the emulsion and compared this to the content of organic solvents in the final particles. We define the yield as the mass of organic solvents (EA, BA, and EtOH) in the oil droplets
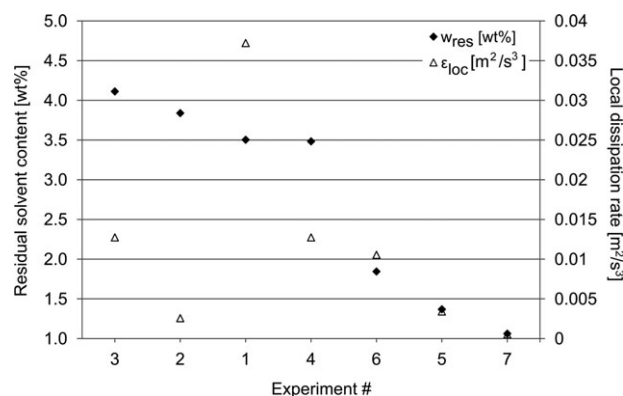

Figure 9. Skeletal density of the microparticles ρ_{sk} and the local dissipation rate at the emulsion injection point ε_{loc} from the flow simulations.

See Tables 2 and 3 for experimental details.

Figure 10. The residual solvent content of the microparticles w_{res} and the local dissipation rates at the emulsion injection point ε_{loc} from the simulations.

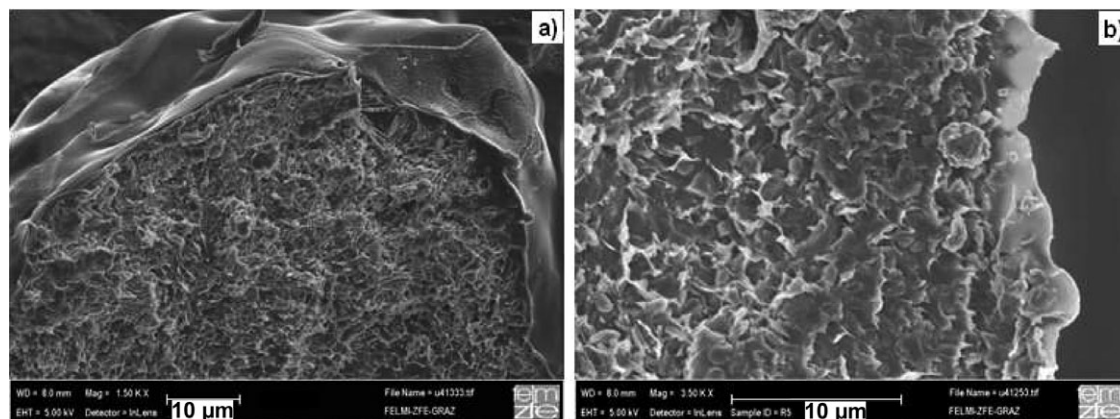See Tables 2 and 3 for experimental details.

Figure 11. Microparticle cross sections from Experiment 6 showing particles covered with a continuous thin layer (a).

This 2–3 μm thick layer and (b) can be related to the PVA stabilizer that covers the oil droplets during oil-in-water emulsification to prevent coalescence.

of the emulsion minus the mass of the same solvents in the final particles, divided by the solvent mass in the oil droplets. The values we obtain in the seven experiments are all close to 1, between 0.9904 and 0.9976, indicating that the yield of the extraction process is very high.

Particle morphology

To investigate the effect of the process parameters on the particle morphology, electron microscopy pictures were taken with the purpose to analyze the structure of microparticle cross sections in relation to the properties of the liquid flow field near the emulsion injection point in the extraction vessel. It has previously been reported that PVA molecules, which were used as an emulsifier in the O/W emulsification, are strongly bound to the surface of PLGA particles.[28] A general observation was that all microparticles were coated with a 2–3-μm thick PVA layer (Figures 11a, b).

The highest local shear and dissipation rates were achieved in Experiment 1. The influence of fast solvent removal at high shear rates is illustrated in Figure 12. A cross section of a microparticle produced in Experiment 1 is shown in Figure 12a. A higher magnification of the peripheral region can be seen in Figure 12b. Here, we can distinguish between a porous region near the particle core and a 5–20-μm thick nonporous layer on the particle surface. This thick layer is not identical to the PVA layer in Figure 11,

but is rather a result of fast solvent removal which led to early polymer precipitation in the periphery region of the microparticles.[11]

It has been reported that fast extraction of ethyl acetate can induce not only early interfacial polymer precipitation, but the formation of hollow microspheres.[10] Figure 13 shows cross sections of the microparticles produced in Experiments 2 and 3. It can be seen that the internal porosity of these samples is very heterogeneous. As expected, large hollow regions were formed in the core of the microparticles. Figure 14a shows a particle cross section from Experiment 6. The internal porosity of this sample is completely homogeneous, even at higher magnification (Figure 14b). The surface and internal porosity distribution of polymeric microparticles is directly related to their release behavior.[29] Therefore, differences in the release profile of the microparticles presented in Figures 13 and 14 are to be expected, which will be the topic of future investigations.

Nondimensional representation of the particle properties influenced by the production process parameters

The purpose of the dimensional analysis was to develop empirical relations between process parameters and the resulting specific surface area, skeletal density, residual solvent content, and Sauter mean diameter of the particles. These relations may provide a basis for scale-up and
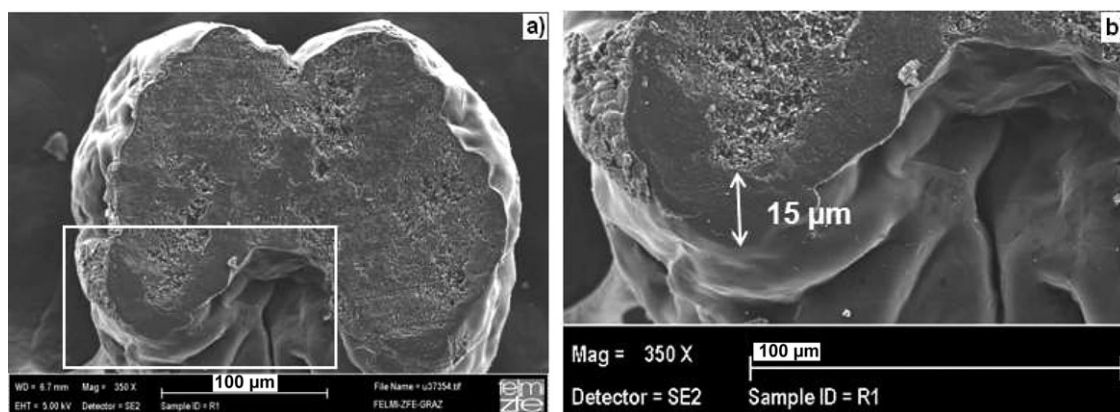

Figure 12. Cross section of a microparticle produced in Experiment 1 showing (a) a heterogeneous porosity distribution and (b) the formation of a 5–20 μm thick nonporous layer in the peripheral region.
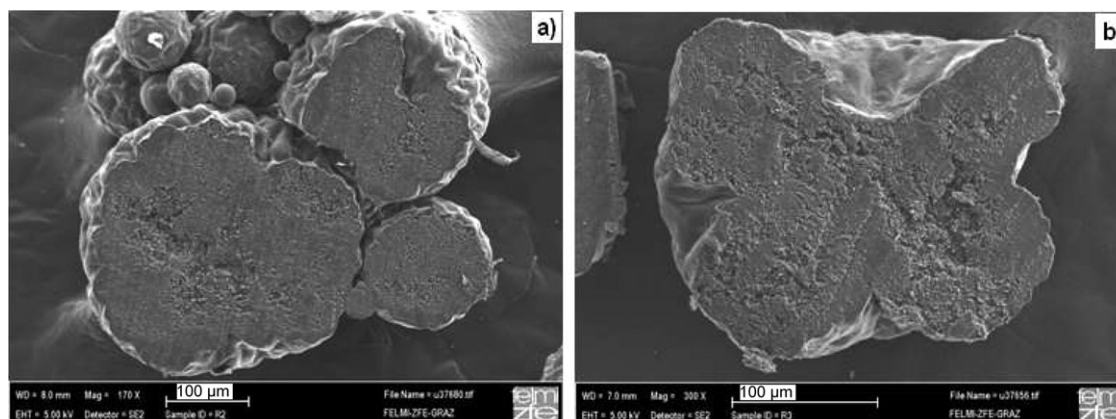
Figure 13. Cross sections of microparticles produced in Experiments (a) 2 and (b) 3 showing heterogeneous porosity with hollow regions.

optimization of the process. Parameters that were considered relevant for the extraction process step were discussed above.

The coefficients B, E, H, and N, and the exponents c, d, f, g, k, m, p, and q of the model Eq. 2–5 were determined by nonlinear regression fitting of the equations to the particle characterization results described in the previous sections. The microparticle charges were produced by the formulations described in Table 1.

In analyzing the dependencies of the final particle properties on the various relevant parameters of the process and material properties, it is not obvious from the beginning whether local or global properties of the turbulent flow field in the reactor are dominant. The measured data above, however, suggest a dominance of local flow properties.

The injection velocity of the emulsion into the extraction medium depends on the oil droplet size in the emulsion required. Typical velocities are 0.05–0.1 m/s. In contrast, local mean velocities of the extraction medium are of the order of some m/s. Typical relaxation times of the oil droplets in the emulsion after injection into the extraction medium are O(1 ms), so that convective mass transfer during the extraction process may be due to the fluctuations in the velocity field only. In all of our experiments, the oil droplets and particles are too large and heavy to follow all the fluctuations of the velocity in the extraction medium. Therefore, they feel those fluctuations and exhibit their effect on mass transfer. The macromixing in the reactor after the injection of the emulsion is determined by the rate of dissipation of the turbulent kinetic energy and given by the Corrsin relation.[30] The macromixing times are of the order of 1 s or less. In comparison with the total batch time of 20 h, this is again a very short time, so that the particles are transported through the whole reactor volume. This could be a reason to expect volume-mean properties of the flow field in the batch reactor to determine the particle properties. We will show below that, despite the present time-scale arguments, the particle properties are rather dominated by local flow field properties. One potential explanation for this surprising result may be a short time scale of particle surface formation.

Determining the dependencies of the specific particle surface on the influencing quantities, it turned out that A_{spec} correlates well with the local rate of turbulent kinetic energy dissipation, ε_{loc}. The correlation, which is shown in Figure 15a, reads

$$\frac{A_{spec}\mu}{\varepsilon_{loc}^{1/3} d_{32,oil}^{1/3}} = 6Sc^{1.26}\left(\frac{\varepsilon_{loc} d_{32,oil}^4}{D^3}\right)^{-0.417} \tag{14}$$

The equation indicates that A_{spec} depends on the Schmidt number of the extraction medium and, of course, on the initial Sauter mean oil droplet size in the emulsion. The
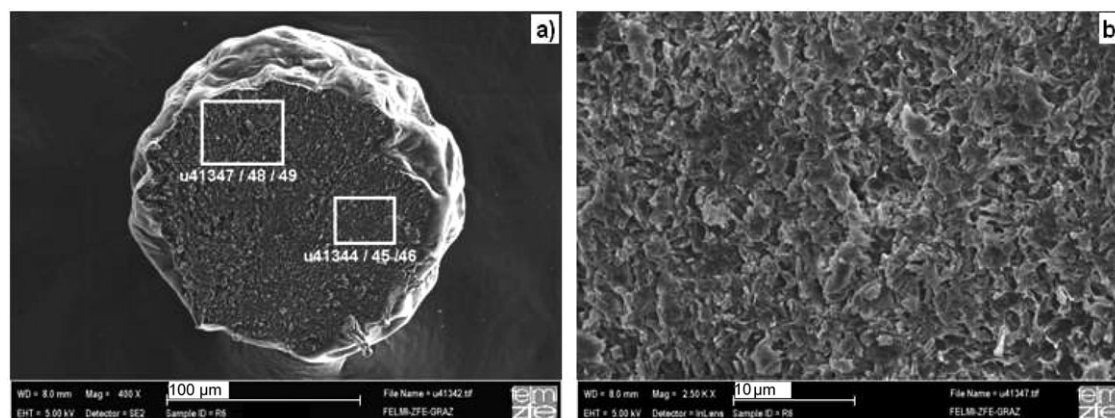

Figure 14. Cross section of a particle from Experiment 6, showing a homogeneous polymer matrix (a) even at higher magnification (b).
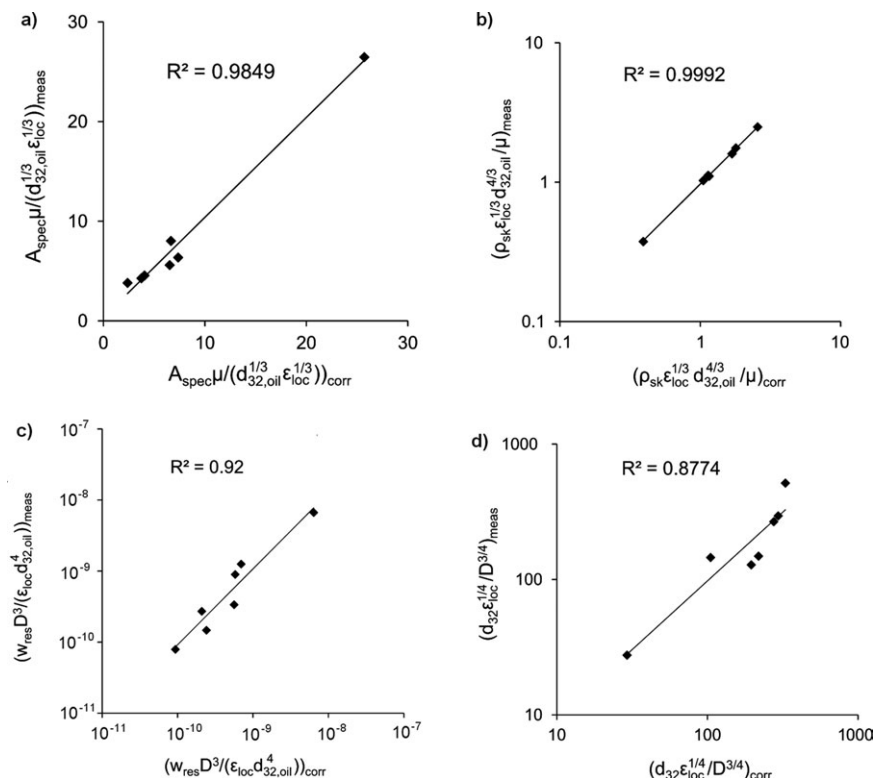
Figure 15. (a) Nondimensional specific surface area of the microparticles as measured and as obtained from Eq. 14, (b) nondimensional skeletal density of the microparticles as measured and as obtained from Eq. 15, (c) residual solvent content in the microparticles in wt% as measured and as obtained from Eq. 17, and (d) particle size of the microparticles as measured after the extraction step and as obtained from Eq. 18.

importance of the local turbulent property of the flow field is interesting to note, because it is not *a priori* clear in which stage of the particle life time A_{spec} is determined. The present result suggests that the specific particle surface is formed in the early stages of particle formation.

The next particle property of interest for API transport is the skeletal density. For this property, the relation

$$\frac{\rho_{sk}\varepsilon_{loc}^{1/3}d_{32,oil}^{4/3}}{\mu} = 0.9Sc^{-0.95}\left(\frac{\varepsilon_{loc}^{1/3}d_{32,oil}^{4/3}}{D}\right) \quad (15)$$

is obtained from the measured data as a first stage of the result. This relation, which is shown in Figure 15b, may be simplified to yield

$$\frac{\rho_{sk}}{\rho} = 0.9Sc^{0.05} \quad (16)$$

indicating that, under the present experimental conditions, the skeletal density resulting from the particle formation process, comes out as a constant and would vary only with the Schmidt number and density of the extraction medium. Indeed, with the present Schmidt number of 1809, the resulting value of ρ_{sk} is 1307 kg/m³, which deviates from the mean of the values measured in the seven experiments by no more than 3%. The fact that the value of this particle property comes out as a constant indicates that it depends strongly on the properties of the materials which were not varied in our study—the diffusivities inside and outside the particles, and other transport properties of the extraction medium, such as its kinematic viscosity.

One property of the particles, which may strongly impact the use as API carriers, is the residual content of organic solvents used for dissolving the polymer in the organic phase. The correlation found to represent the measured data best reads

$$\frac{w_{res}D^3}{\varepsilon_{loc}d_{32,oil}^4} = 5\cdot10^{-6}Sc\left(\frac{\varepsilon_{loc}d_{32,oil}^4}{D^3}\right)^{-0.75} \quad (17)$$

The dependency of the residual organic solvent content of the particles on a local transport property of the flow field in the extraction medium is not a trivial result. The dependency indicates clearly that, together with the two other structural properties of the particles discussed above, the residual organic solvent content of the particles is determined in the very early phases of the particle formation. As a reason for this phenomenon, one may see the formation of a dense layer of PLGA polymer on the oil droplets right after the start of the extraction process. Despite the long batch time of the extraction, the remainder of organic solvent in the particles is strongly dependent on this very early process which hinders the mass transfer across the particle surface. A reason for the weak correlation seen in Figure 15c may be the influence of the particle washing and drying on the organic solvent content, which is an influence not accounted for in the analysis.

The final property of the particles studied in our article is their Sauter-mean diameter after the extraction step. The correlation obtained, which is shown in Figure 15d, reads

$$\frac{d_{32}\varepsilon_{\text{loc}}^{1/4}}{D^{3/4}} = 0.086 Sc^{-0.54}\left(\frac{\varepsilon_{\text{loc}}d_{32,\text{oil}}^4}{D^3}\right)^{0.52} \quad (18)$$

The relation exhibits the same structure of the right-hand side as the three others above, indicating the importance of mass transfer across the oil droplet (or particle) surface for the particle properties. The dominant mechanism in the convective transport is again turbulence, represented by the rate of dissipation of the turbulent kinetic energy. This correlation is the weakest of the four relations found, because the rate of shrinkage during microparticle hardening and the resulting final particle size depend on the extraction rate. Furthermore, the high stirring speed and the emulsion injection point placed near the blade of the anchor stirrer may cause droplet breakup at the injection tube. This phenomenon leads to reduced particle sizes, which are not entirely predictable and lead to a weak correlation in the dimensional analysis.

The values of the coefficients of determination R^2 are close to unity in all cases. This means that the developed correlations (14)–(18) accurately predict the specific surface area, skeletal density, residual solvent content, and particle size based on the tip speed of the anchor stirrer, oil drop size, local dissipation rate in the liquid flow field, and material properties of the extraction medium.

Conclusions

The influence of process parameters on PLGA-microparticle properties to be used as API carriers has extensively been reported in the literature. The main challenge for optimization and scale-up of the particle production process is to fit all properties of the microparticles to their expected release behaviour. In this work, we carried out experiments and CFD simulations of the particle formation process to describe quantitatively the processes during the emulsion extraction. Using CFD, we quantified the influence of the extraction rate on the porosity and density of the microparticles. Moreover, we accurately predicted the specific surface area, skeletal density, residual solvent content, and the particle size of the final solid microparticles based on the turbulent dissipation rate, local shear rate, oil droplet size, diffusion coefficient of the organic solvent in water, and material properties of the extraction medium. The dependencies of the final particle properties on the various relevant parameters of the process were analyzed using dimensional analysis. The main results and conclusions can be summarized as follows:

- A_{spec} depends on the Schmidt number of the extraction medium, on the initial Sauter mean oil droplet size in the emulsion and, on the local rate of turbulent kinetic energy dissipation, ε_{loc}.
- ρ_{sk} resulting from the particle formation process, comes out as a constant and would vary only with the Schmidt number and density of the extraction medium.
- w_{res} strongly depends on the local transport property of the flow field in the extraction medium.
- d_{32} depends on the Schmidt number of the extraction medium, on the initial Sauter mean oil droplet size in the

emulsion and on the rate of dissipation of the turbulent kinetic energy.

The results of the present study suggest that the particle properties are rather dominated by local flow field properties. One potential explanation for this surprising result may be a short time scale of particle surface formation. Furthermore, the convective mass transfer across the oil droplet surface is dominated by turbulence, represented by the local rate of turbulent kinetic energy dissipation, ε_{loc}. It was clearly demonstrated that the local values of these quantities at the emulsion injection point are crucial regarding the final particle properties.

The achievement of the developed correlations consists in the account for process variables calculated by simulations of the flow field in the extraction vessel. The results are useful for predicting microparticle properties produced in reactors of any geometry using any type of stirrer, also on larger scales.

Literature Cited

1. Wischke C, Schwendeman S. Principles of encapsulating hydrophobic drugs in PLA/PLGA microparticles. *Int J Pharm*. 2008;364:298–327.
2. Jyothi N, Prasanna P, Sakarkar S, Prabha K, Ramaiah P, Srawan G. Microencapsulation techniques, factors influencing encapsulation efficiency. *J Microencapsulation*. 2010;27:187–197.
3. Freitas S, Merkle H, Gander B. Microencapsulation by solvent extraction/evaporation: reviewing the state of the art of microsphere preparation process technology. *J Controlled Release*. 2005;102:313–332.
4. Kiss N, Brenn G, Pucher H, Wieser J, Scheler S, Jennewein H, Suzzi D, Khinast J. Formation of O/W emulsions by static mixers and production of microparticles for pharmaceutical applications. *Chem Eng Sci*. 2011;66:5084–5094.
5. Jeyanthi R, Mehta R, Thanoo B, DeLuca P. Effect of processing parameters on the properties of peptide-containing PLGA microspheres. *J Microencapsulation*. 1997;14:163–174.
6. Mao S, Xu J, Cai C, Germershaus O, Schaper A, Kissel T. Effect of WOW process parameters on morphology and burst release of FITC-dextran loaded PLGA microspheres. *Int J Pharm*. 2007;334:137–148.
7. Freiberg S, Zhu X. Polymer microspheres for controlled drug release. *Int J Pharm*. 2004;282:1–18.
8. Yeo Y, Park K. Control of encapsulation efficiency and initial burst in polymeric microparticle systems. *Arch Pharm Res*. 2004;27:1–12.
9. Klose D, Siepmann F, Elkharraz K, Krenzlin S, Siepmann J. How porosity and size affect the drug release mechanisms from PLGA-based microparticles. *Int J Pharm*. 2006;314:198–206.
10. Sah H. Microencapsulation techniques using ethyl acetate as a dispersed solvent: effects of its extraction rate on the characteristics of PLGA microspheres. *J Controlled Release*. 1997;47:233–245.
11. Li W, Anderson K, Mehta R, DeLuca P. Prediction of solvent removal profile and effect on properties for peptide-loaded PLGA microspheres prepared by solvent extraction/evaporation method. *J Controlled Release*. 1995;37:199–214.
12. Vay K, Scheler S, Friess W. New insights into the pore structure of Poly (D, L-lactide-co-glycolide) microspheres. *Int J Pharm*. 2010;402:20–26.
13. Jeyanthi R, Thanoo B, Metha R, DeLuca P. Effect of solvent removal technique on the matrix characteristics of polylactide/glycolide microspheres for peptide delivery. *J Controlled Release*. 1996;38:235–244.
14. Su Z, Sun F, Shi Y, Jiang C, Meng Q, Teng L, Li Y. Effects of formulation parameters on encapsulation efficiency and release

behavior of risperidone poly (D, L-lactide-co-glycolide) micro-sphere. *Chem Pharm Bull.* 2009;57:1251–1256.

15. Zlokarnik M. *Scale-up—Modellübertragung in der Verfahrenstechnik,* 2nd ed. Weinheim (Germany): Wiley-VCH Verlag GmbH & Co. KGaA, 2005.

16. AVL List GmbH, AVL FIRE (R) CFD Solver Manual v 2009, vol. 2009, ed. 04, rev. B, AVL List GmbH, Graz, Austria, 2009.

17. Hörmann T, Suzzi D, Khinast JG. Mixing and dissolution processes of pharmaceutical bulk materials in stirred tanks: experimental and numerical investigations. *Ind Eng Chem Res.* 2011;50:12011–12025.

18. Hanjalic K, Popovac M, Hadziabdic M. A robust near-wall elliptic-relaxation eddy-viscosity turbulence model for CFD. *Int J Heat Fluid Flow.* 2004;25:1047–1051.

19. Durbin PA. Near-wall turbulence closure modeling without "damping functions". *Theor Comput Fluid Dyn.* 1991;3:1–13.

20. Dukowicz JK. *Quasi-steady droplet phase change in the presence of convection.* Informal Report, LA 7997-MS, Los Alamos Scientific Laboratory, 1979.

21. Armenante PM, Kirwan DJ. Mass transfer to microparticles in agitated systems. *Chem Eng Sci.* 1989;44:2781–2796.

22. Levins DM, Glastonbury JR. Application of Kolmogoroff's theory to particle-liquid mass transfer in agitated vessels. *Chem Eng Sci.* 1972;27:537–543.

23. Perry RH, Green DW, Maloney JO. *Perry's chemical Engineers' Handbook,* 7th ed. New York: The McGraw-Hill Companies Inc., 1999.

24. Lal P, Kumar S, Upadhyay SN, Upadhya YD. Solid-liquid mass transfer in agitated Newtonian and non-Newtonian fluids. *Ind Eng Chem Res.* 1988;27:1246–1259.

25. Hamishehkar H, Emami J, Najafabadi A, Gilani K, Minaiyan M, Mahdavi H, Nokhodchi A. The effect of formulation variables on the characteristics of insulin-loaded poly (lactic-co-glycolic acid) microspheres prepared by a single phase oil in oil solvent evaporation method. *Colloids Surf B.* 2009;74:340–349.

26. Katou H, Wandrey A, Gander B. Kinetics of solvent extraction/evaporation process for PLGA microparticle fabrication. *Int J Pharm.* 2008;364:45–53.

27. Li M, Rouaud O, Poncelet D. Microencapsulation by solvent evaporation: state of the art for process engineering approaches. *Int J Pharm.* 2008;363:26–39.

28. Murakami H, Kobayashi M, Takeuchi H, Kawashima Y. Preparation of poly (DL-lactide-co-glycolide) nanoparticles by modified spontaneous emulsification solvent diffusion method. *Int J Pharm.* 1999;187:143–152.

29. Yang Y, Chung T, Bai X, Chan W. Effect of preparation conditions on morphology and release profiles of biodegradable polymeric microspheres containing protein fabricated by double-emulsion method. *Chem Eng Sci.* 2000;55:2223–2236.

30. Edward LP, Atiemo-Obeng VA, Kresta SM, editors. *Handbook of Industrial Mixing: Science and Practice.* NJ, USA: Wiley Hoboken, 2004.